Chapter 3

Li^+ ion conducting NASICON reinforced hybrid polymer composites

As a novel approach, in this chapter, the effect of Li^+ NASICON (LTP & LATP) dispersion on electrical, thermal and structural properties in PEO-$LiCF_3SO_3$ composites is discussed thoroughly.

The Chapter demonstrates that in an appreciably wide range of compositions, electrical conductivity exhibits a systematic rise. This is unlike the case of composites with insulating nano-fillers where conductivity drops above a certain content of fillers in the matrix.

The chapter presents separate conductivity estimation for different phases in composites, i.e. polymer, LTP/LATP, and polymer at LTP/LATP grain boundaries and collects evidences of role active fillers in facilitating electrical transport.

The overall mechanism, however, will be presented in a separate chapter after establishing conductivity-structure correlation.

(a) M.D. Singh, B. Nayak, B. Choudhury, A. Sarit, A. Dalvi, *Li^+-NASICON crystallites in PEO-$LiCF_3SO_3$ matrix: Characterization of a novel hybrid electrolyte*, Solid State Ionics. 311 (2017) 20-25.

(b) M. D. Singh, A. Dalvi, D M Phase, Y. Kumar, *"$Li_{1.3}Al_{0.3}Ti_{1.7}(PO_4)_3$ reinforced hybrid polymer composites: Assessment of enhanced Li^+ ion transport and potential for solid state supercapacitor applications"*, *J. Mat. Science*, 55 (2020) 3951–3963

3.1. PEO-$LiCF_3SO_3$-LTP system

In the current section, the samples under discussion are $95[PEO_{1-x}LTP_x]$-$5LiCF_3SO_3$ where $0 \leq x \leq 0.9$. Composites with x = 0 - 0.9 are abbreviated as 0 LTP - 90 LTP, respectively.

3.1.1 X-ray diffraction

The XRD measurements (Fig. 3.1) were performed on flat films ($x \leq 0.4$). Dissolution of the salt leads to amorphous phase formation in the polymer matrix that is evident due to suppressed peaks of crystalline PEO [1][2]. As evident, pristine PEO and polymer composite 0 LTP appears to exist in a mixed phase. As LTP content increases, the O/Li ratio decreases. For example, x = 0.8 corresponds to approximate O/Li ratio of 13:1, and x = 0 to 67:1. Thus for a wide range of O/Li ratio salt completely dissolves in the matrix, as there is no evidence of peaks corresponding to $LiCF_3SO_3$.

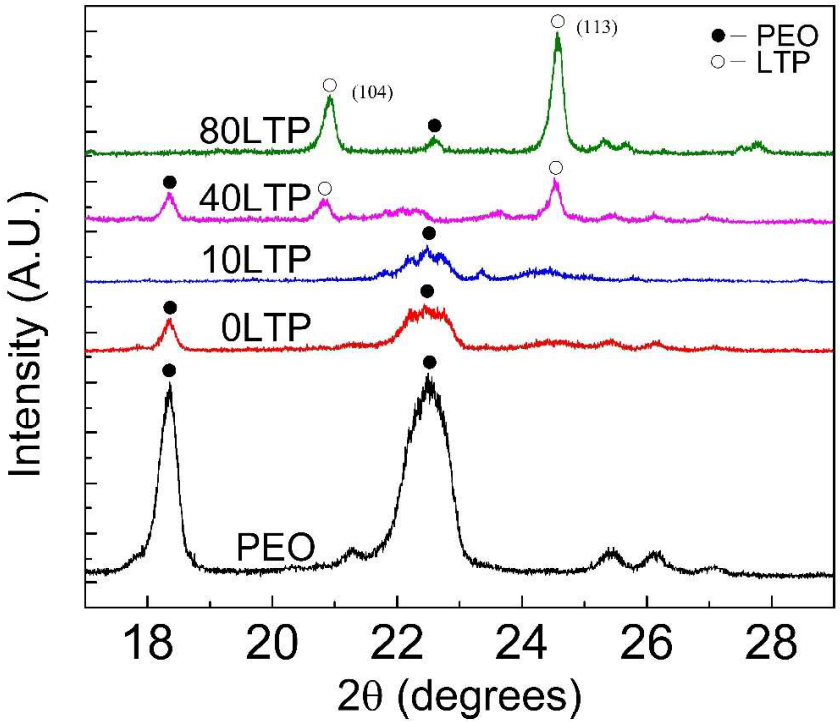

Figure 3.1 *X-ray diffraction patterns for samples 0-80 LTP. Index as per* [3].

With a gradual increase of LTP, finally, it is possible to obtain a composition, 80LTP, in which LTP exists with 76 wt% and occupies a large volume fraction of the matrix. Further, it is evident that no new crystalline phase forms during composite formation. It is also possible to

obtain a composition with x = 0.9 (90 LTP). Nevertheless, such a dispersion leads to segregation. XRD results also suggest that LTP particles do not lose their structure during the synthesis and exist in a separate phase when reinforced in the polymer matrix.

3.1.2. Differential scanning calorimetry

The DSC thermograms for the composites are shown in Fig. 3.2a. The heat flow (y-axis) is normalized with respect to amount of PEO in the sample. For pristine PEO as well as 0 LTP, a broad endothermic peak onset appears at ~ 57°C that may be attributed to the melting event of the host polymer as also reported earlier [4][5]. With LTP addition the area under the peak gradually decreases, that suggests suppression of PEO melting [6][1]. These DSC thermograms have been used to obtain enthalpies and degree of crystallinity in PEO according to following relation [1]:

$$\text{Fraction of crystallinity} = \frac{\Delta H_{CPE}}{\Delta H_{Polymer}} \times 100 \qquad (1)$$

where ΔH_{CPE} and $\Delta H_{polymer}$ are melting enthalpies of PEO in polymer composite and pristine PEO (Alfa Aesar; M.W. = 300,000), respectively.

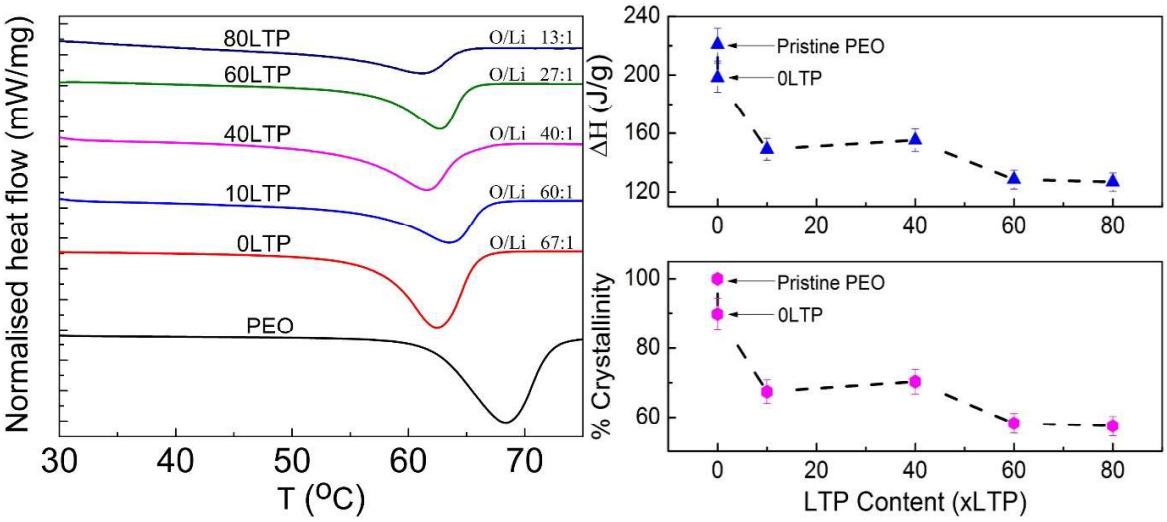

Figure 3.2 *(a) DSC thermograms (heat flow is normalized w.r.t. PEO amount in each composition) for the solid polymer composites with various LTP content. Approximate O/Li ratio is also given for each sample. (b) PEO Crystallinity as a function of LTP content.* ΔH^0_m *is the actual melting enthalpy as obtained from the DSC experiment for pristine PEO. Pristine PEO crystallinity is considered 100% and used as a reference to define other crystallinities* [1].

Thus for all the samples enthalpies (in J/g) and % crystallinities were calculated and plotted in Fig. 3.2b. The enthalpy content as well as crystallinity of PEO decreases initially rapidly and does not show much drop at high LTP contents. Though 80LTP sample also exhibits a subtle endothermic dip in the DSC thermogram, but certainly corresponds to the lowest crystallinity of ~ 57%. Primarily, the change in O/Li ratio is known as a responsible factor for the decrease in the crystallinity as revealed earlier [7]. In addition, as also suggested previously, addition of fine insulating [6] as well as conducting particles [8] in the polymer matrix do promote localized amorphous regions. Thus in the present case (i) active filler (LTP) addition and (ii) decrease of polymer to salt ratio, both may contribute to amorphization of the polymer matrix.

3.1.3. Electrical properties

The electrical conductivity is measured on hybrid polymer films ($x \leq 0.4$) and pellets ($x > 0.4$). Since a compressed polymer may further relax with time, the pellets (prepared from vacuum dried slurry) were kept at room temperature for ~ 7 day before measurement of electrical properties. Whereas, the films were vacuum dried at 40 °C prior to conductivity cycles to remove the stresses. In the inset of Fig. 3.3, the images of film of 40 LTP and pellet of 90 LTP are shown. The films were found to be flexible in nature. Further, the pellets were found to be compact, dense and mechanically stronger.

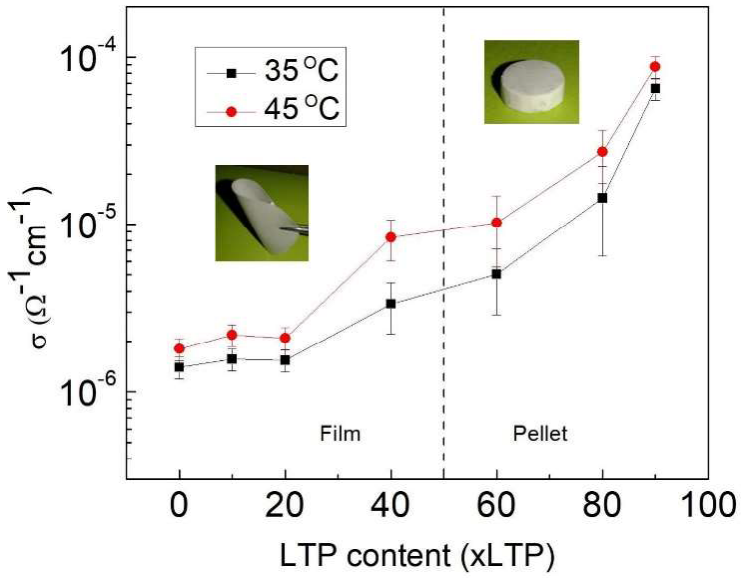

Figure 3.3 *Electrical conductivity (1kHz) as a function of LTP content. (For $x \leq 0.4$ polymer films; $x > 0.4$ pellets). Inset shows images of (i) 40 LTP film and (ii) 90 LTP pellet of diameter 8 mm.*

The electrical conductivity (1 kHz) variation with LTP content is shown in Fig. 3.3 at two different temperatures in the thermally stable region. As evident, initially it does not exhibit any appreciable variation with LTP content. However, for higher contents (x > 0.2), a significant rise in conductivity is witnessed. Interestingly, for very high LTP content (x = 0.8 & 0.9), when the amount of polymer in the composite is low the conductivity approaches a value of ~ 10^{-4} $\Omega^{-1}cm^{-1}$, that is close to the in-grain conductivity of Li^+-NASICON crystallites as reported by many workers [9]. At 60°C highest conductivity of 1.7×10^{-4} $\Omega^{-1}cm^{-1}$ is achieved for 90LTP sample. Such a large variation in conductivity suggests that the active filler grains may provide pathways for Li^+ ions to contribute in electrical transport.

To investigate the stability of conductivity with respect to thermal cycling its temperature dependence (1°C/min) is plotted for all chosen compositions (Fig. 3.4).

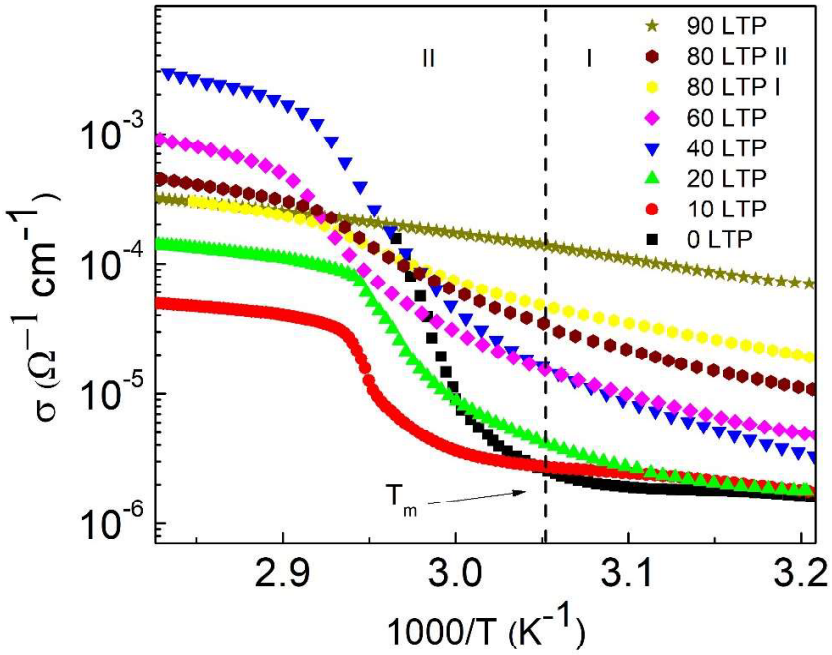

Figure 3.4 *Electrical conductivity-temperature cycles obtained at 1kHz for polymer composite samples with various LTP content. (For x ≤0.4 polymer films; x > 0.4 pellets). 80 LTP-I and II refer to the first and second heating cycles of 80LTP sample.*

As apparent, conductivity exhibits very interesting trends. For lower LTP content samples, conductivity increases Arrheniusly and exhibits a notable rise at ~ 57-60°C i.e. at the melting onset of PEO. Interestingly when the LTP substitutes PEO, the melting event gradually

becomes less prominent. Thus, the variation (deviation from Arrehenius behavior) of electrical conductivity at melting point (T_m) also appears less evident possibly due to the smaller amount of PEO in the matrix. Apparently for very high LTP content, 80-90LTP, polymer melting does not affect the conductivity, and Arrhenius behavior is witnessed for a fairly wide range of temperature (even $T >> T_m$). To further understand the thermal stability of hybrids, a second heating cycle of 80LTP was performed. A subtle fall in the conductivity at room temperature is noticed after the first cycle. However, the second heating cycle (80LTP-II) was found to be nearly reproducible in a wide temperature range (30-130°C). This in turn suggests that composites with a large amount of LTP can apparently withstand wide temperature variation, therefore exhibit appreciable thermal stability.

In order to get further insights into electrical transport, conductivity spectra (steady-state) were obtained in a wide range of frequency (4 Hz–5 MHz) for the composites in the shape of films ($x \leq 0.4$) and pellets ($x > 0.4$). From conductivity isotherms, it is possible to resolve different contributions (from bulk, grain boundary) as described by various researchers [10–12]. The σ-ω plots for samples with large LTP content (pellets) are shown in Fig. 3.5b and c. Apparently, the trend of the conductivity spectra is significantly different than those of low LTP content samples (Fig. 3.5a). For these, two apparent plateaux are witnessed that suggest a contribution of LTP crystallites in electrical transport. For the pellet samples since LTP content is high, the low frequency plateau conductivity is mainly due to long range migration of ions and it may have two important contributions viz. motion of ions through (i) compressed polymer chains existing at the grain-grain interfaces and (ii) from the grain boundaries of LTP where polymer could not reach. It is tricky to estimate separate contributions of these components thus a combined contribution for long range migration of ions is taken as polymer-grain boundary conductivity (σ_{PGB}). The high frequency plateau may be attributed to localized motion of ions. It is plotted on an extended scale in the inset of Fig. 3.5b and c for clarity. The value of bulk conductivity is inferred from this plateau and plotted with temperature (Fig.3. 6b). The activation energy corresponding to the conductivity interestingly matches well with that of pristine LTP (0.20-0.30 eV) thus considered in-grain conductivity of LTP. This value is approximated from the onset of high frequency dispersion and considered as in-grain conductivity of LTP (σ_{LTP}) as shown in Fig. 3.6b.

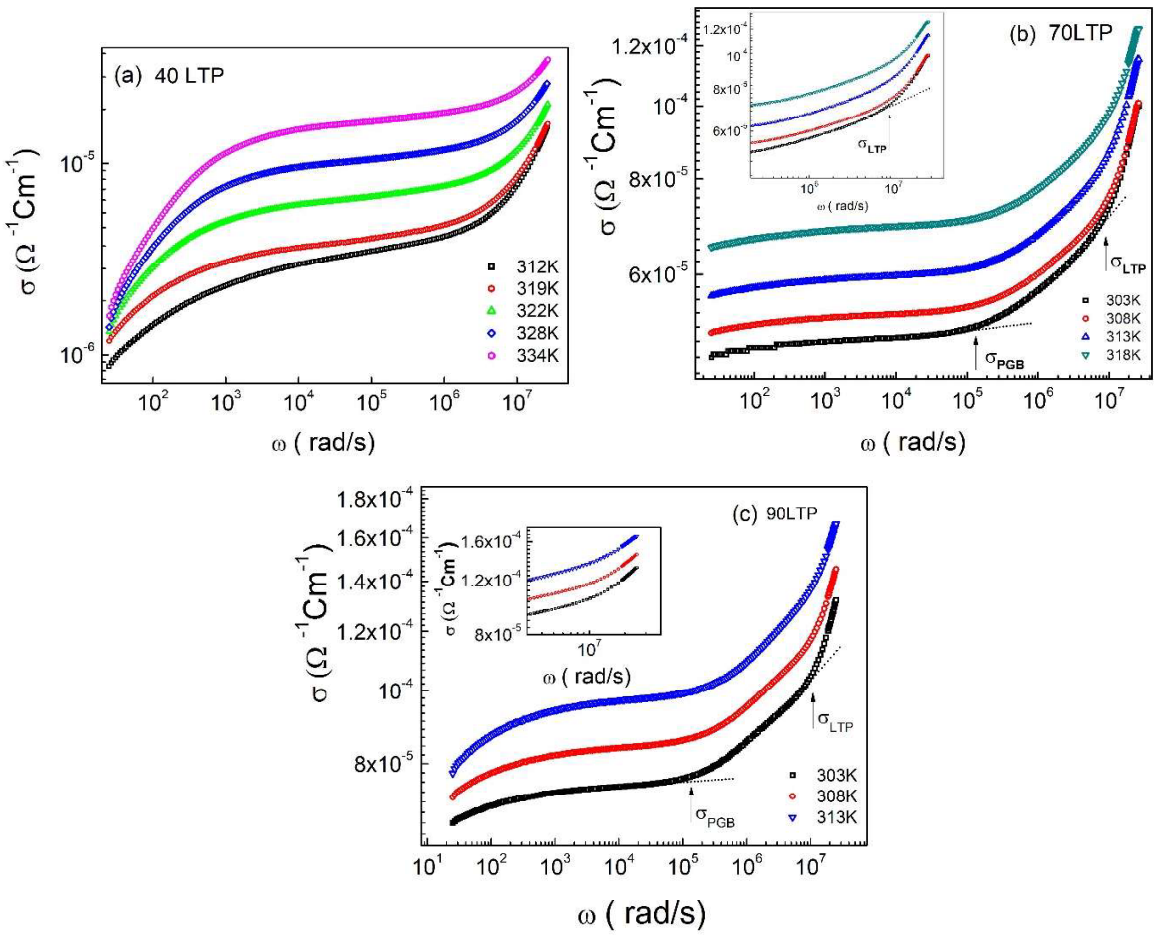

Figure 3.5 *Electrical conductivity versus frequency for samples with (a) 40 LTP, (b) 70 LTP, and (c) 90 LTP content. Inset of b and c shows the apparent dc to dispersion in high frequency region.* σ_{LTP} *is calculated from the onset of this dispersion.*

Thus estimation of in-grain (σ_{LTP}) and polymer-grain boundary conductivity (σ_{PGB}) values has been made from σ-ω plots and plotted with temperature in Fig. 3.6a and b. Evidently, both the conductivities increase almost linearly with temperature. They also exhibit an appreciable rise with increasing LTP content. The reason for the increase of σ_{PGB} with increasing LTP content could be attributed to a possible increase in the density of the pellets. An increase of LTP content reduces the polymer content and improves the density, mechanical strength of the pellets. Further, decrease of O/Li ratio also provides good Li^+ ion concentration at the interface. Though polymer content is small, it is still useful to keep the salt at interface in

ionized state. The bulk conductivity (σ_{LTP}) rise should be owing to the fact that LTP occupies a gradually larger volume fraction and thus dominates the bulk property.

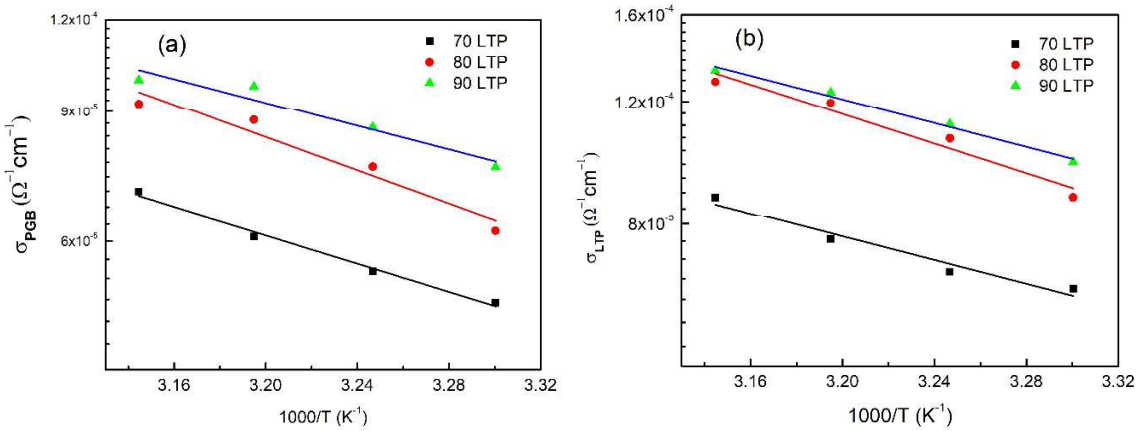

Figure 3.6 *Temperature dependency of electrical conductivity for high LTP content samples. (a) Polymer-grain boundary conductivity (σ_{PGB}) and (b) bulk conductivity (σ_{LTP}).*

To initiate a discussion of whether electrical transport is facilitated by NASICON crystallites, a comparative conductivity-temperature plot (Fig. 3.7) is also shown for a fixed O/Li ratio of 13:1. A well-known analogue of LTP is LATP ($Li_{1.3}Al_{0.3}Ti_{1.7}(PO_4)_3$) that exhibits better electrical transport than LTP [13].

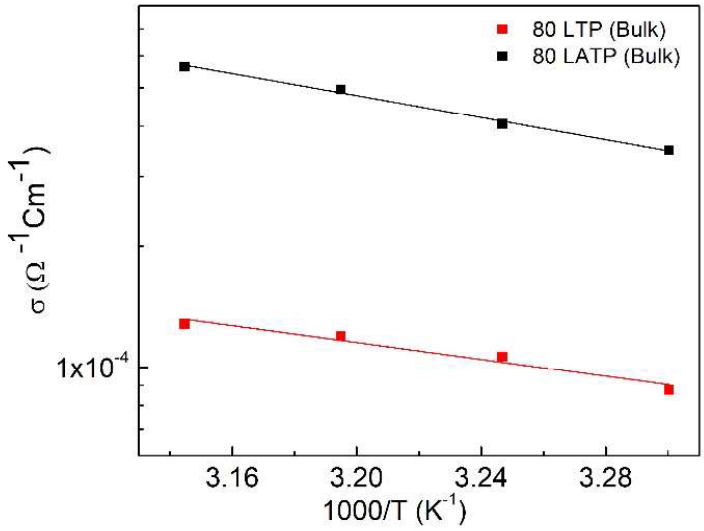

Figure 7. *Arrhenius plot for fixed O/Li ratio of 13:1 for 80LTP and its analogue 80LATP hybrid.*

Thus LTP was substituted with LATP in the matrix and bulk contributions were compared. The bulk conductivity of LATP dispersed sample (80LATP) exhibits significant enhancement. It readily suggests that dispersed active filler particles play a major role in providing conductivity pathways. Since LATP based composites are based on a superior analoque of LTP and also exhibit better conductivity, the subsequent discussion is shifted to LATP composites.

3.2 PEO-$LiCF_3SO_3$-LATP system

Samples under discussion are $5LiCF_3SO_3$-$95[PEO_{1-x}LATP_x]$ where $0 \leq x \leq 0.7$, and composition $Li_{1.3}Al_{0.3}Ti_{1.7}(PO_4)_3$ term as LATP. In the further discussion, the compoite with x = 0 will be abbreviated as 0 LATP, and similary x = 0.1 as 10 LATP and so on upto x = 0.7 as 70 LTP.

3.2.1 X-ray diffraction and Differential Scanning calorimetry

Fig. 8 shows the XRD patterns for 0, 20, 40 and 70 LATP hybrids. Peaks corresponding to LATP and PEO are evident. The peak positions of embedded LATP crystallites match quite well with the earlier findings [14][15][16], i.e. a typical hexagonal structure with lattice parameters a = 8.51Å and c = 20.84Å. Further, size of LATP crystallites is calculated to be ~ 30 nm using Debye Scherer relation. Interestingly, salt in all composites remained completely dissolved and, the peaks corresponding to PEO appear to be suppressed as well as broadened when LATP is gradually added to the matrix. The PEO peak positions also shift marginally that suggests strain/stress introduced due to the LATP addition. The Scherrer length [17], a measure of crystallite size of PEO, gradually decreases from 12.8 nm for 0LATP to 8.40 nm for 70 LATP.

The Inset of Fig. 8 shows DSC patterns wherein PEO melting (endothermic dip) is prominently seen. As observed (Similar to LTP-polymer hybrids), the area under the endothermic dip gradually reduces with increasing LATP, and suppresses significantly for higher content. These, in turn, again suggest a significant reduction in crystalline fraction of PEO due to LATP addition, as also complemented by X-ray diffraction.

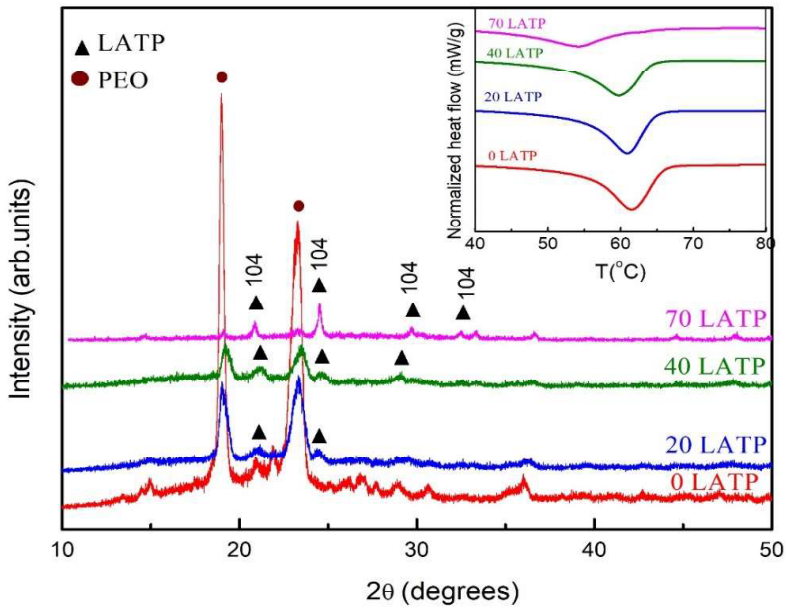

Figure 3.8 *XRD patterns for 0 LATP, 20 LATP, 40 LATP and 70 LATP hybrid CPEs. Inset shows DSC thermograms of hybrid CPEs viz. 0 LATP, 20 LATP, 40 LATP and 70 LATP. Indexing as per ref* [115]. *Similar to LTP-composites, crystallinity gradually decreases with LATP addition.*

3.2.2 Field emission scanning electron microscopy (FESEM):

Surface morphology and elemental distribution in the composites were studied using FESEM. Fig. 9a, b and c depict the FESEM images for composites 0 LATP, 40 LATP and 70 LATP, respectively. As seen, LATP nanoparticles are quite homogeneously embedded into the polymer matrix (Fig. 3.9b). For 70 LATP (Fig. 3.9c) the active filler particles are in significant amount and visible more prominently. Further, the polymer appears to exist between these tiny LATP grains of uniform size.

Elemental distribution of the composite was obtained from EDS spectra of 0 LATP, 40 LATP and 70 LATP content. EDS mapping image for 70 LATP sample is shown in Fig. 3.9d. As evident, an even distribution of elements corresponding to salt (S, F) and NASICON nanoparticles (P, Ti) in the composites is observed (Fig. 3.9d and e). FESEM thus suggests no agglomeration/segregation of elements in the matrix.

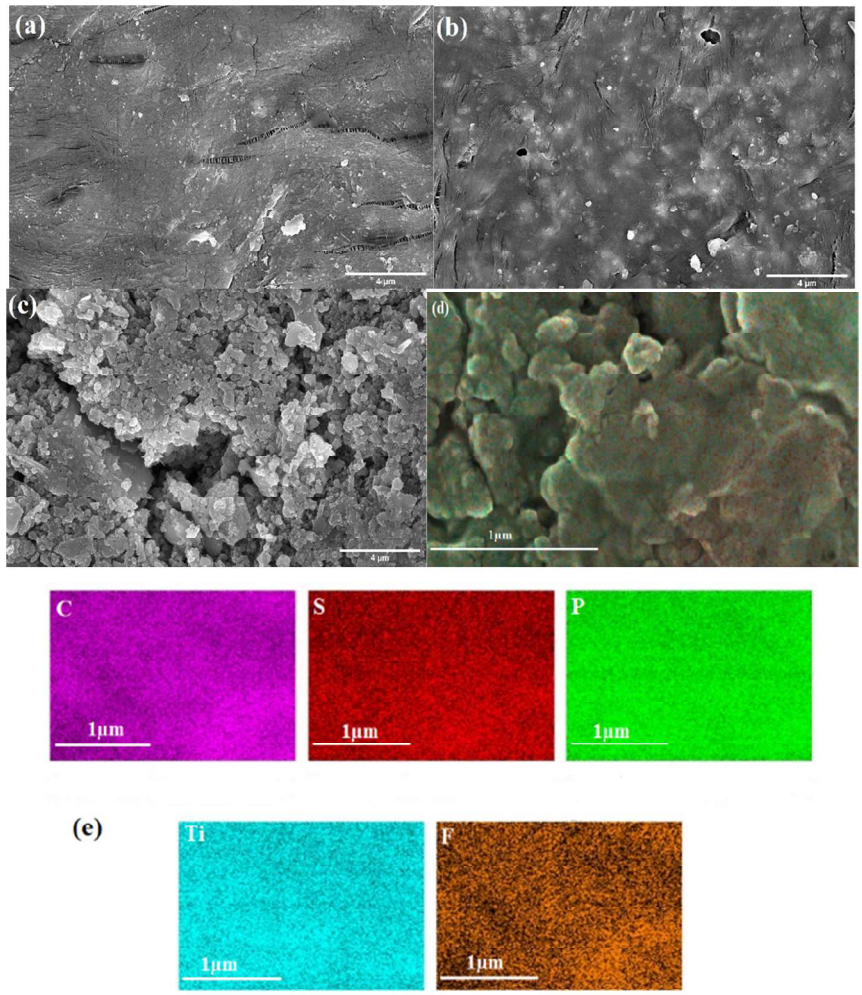

Figure 3.9 *FESEM images of the composites a 0 LATP b 40 LATP and c 70 LATP. d EDS mapping image for 70 LATP sample. e Elemental distribution of C, S, P, Ti and F for 70 LATP sample.*

3.2.3Electrical Characterization:

The frequency dependent electrical conductivity for the composites obtained from the ac impedance spectra was investigated thoroughly. Fig. 3.10 depicts the well-fitted Nyquist plots as obtained for samples with high (70 LATP) and moderate (for 40 LATP, inset) active filler content at various temperatures.

As noticed, an inclined line at a lower frequency (due to ionic polarization) followed by a depressed semicircle at higher frequencies is observed in both the cases. Importantly, the semicircle intercept to x-axis is evidently shifted away from origin for 70 LATP, due to which

the two systems in Fig. 3.10 can be modeled differently (inset of Fig. 3.10). For 70 LATP, the high frequency intercept at X-axis corresponds to a resistance R_1 that may be attributed to bulk transport in LATP. Since LATP exists in a large amount, the contribution of grains to facilitate conductivity is detectable. On the other hand, evident semicircle for 70 LATP may correspond to long range diffusion process, therefore, inter-grain transport. Since for such high filler content, polymer is expected to be present at LATP grain-grain interface, the corresponding conductivity may be attributed to polymer-grain boundary contribution (hereafter PGB).

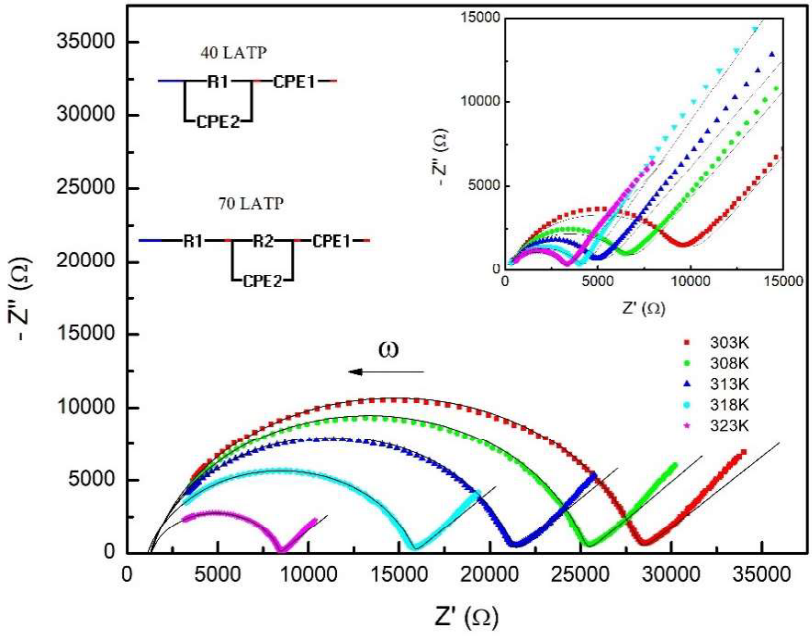

Figure 3.10 *Nyquist plot for Ag|0LATP|Ag cell configuration at different temperatures. Inset shows (i) the same for 40 LATP at different temperatures and (ii) corresponding equivalent circuits for 40 and 70 LATP.*

For 40 LATP (and hence lower LATP content samples), it is rather tricky to accurately calculate the contribution of different phases due to a small volume fraction of LATP crystallites. The semicircle at low frequencies terminates almost at the origin. Therefore in absence of apparent contribution from LATP, the semicircle (inset Fig. 3.10) is attributed mainly to polymer bulk.

Interestingly, for 70 LATP, one can separate out the contribution of two phases namely, (i) LATP and (ii) PGB, therefore σ_{LATP} (from R1) and σ_{PGB} (from R2) are obtained and plotted in

Fig. 3.11a. As shown, the σ_{LATP} approaches to ~ 10^{-3} $\Omega^{-1}cm^{-1}$ at room temperature with an activation energy of ~ 0.49 eV that is in agreement with reported values for bulk/in-grain contribution of LATP [18]. The σ_{PGB} is found to be about one order of magnitude less, and also exhibited a slight deviation from Arrhenius behavior at the initiation of the melting event of the polymer phase (T_m).

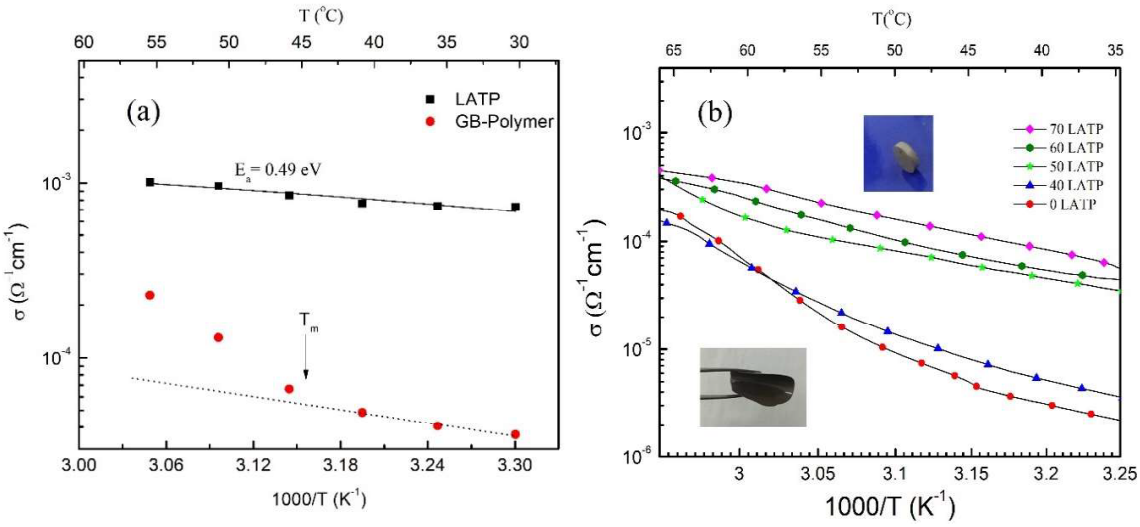

Figure 3.11 *(a) For 70 LATP, the temperature dependence of ionic conductivity of components, viz. polymer–grain boundary (σ_{PGB}) and LATP grains (σ_{LATP}). (b) Total ionic conductivity versus temperature for 0–70 LATP samples.*

Temperature dependence of total conductivity (obtained from total resistance in Nyquist plot) for a wide range of composition is plotted in Fig. 3.11b. For low LATP content, the conductivity deviates at T_m. Nevertheless, as suggested by DSC scans for 60 and 70 LATP (inset, Fig 3.8a), such a deviation is less prominent thus polymer melting does not affect linear behavior of conductivity even at for $T \geq T_m$.

With LATP addition, total conductivity (30°C) shows no prominent rise up to 30 LATP. However, for higher contents, noticeable rise is evident and a maximum conductivity of ~ 10^{-4} $\Omega^{-1}cm^{-1}$ is achieved at 45°C for 70 LATP. Importantly, the conductivity for samples in pellet shape was observed for ~ 6 months and found to be nearly constant.

To understand the electrical transport mechanism, conductivity scaling behavior is observed with compositional and temperature variation. For 70 LATP, with temperature, a good scaling is observed (Inset: Fig. 3.12), which readily suggests no change in the ionic transport mechanism. However, the same (Fig. 3.12) for varied LATP content is completely missing, that may be attributed to an apparent change in the mechanism. In other words, pathways provided by LATP grains appear to play a crucial role in the conductivity mechanism.

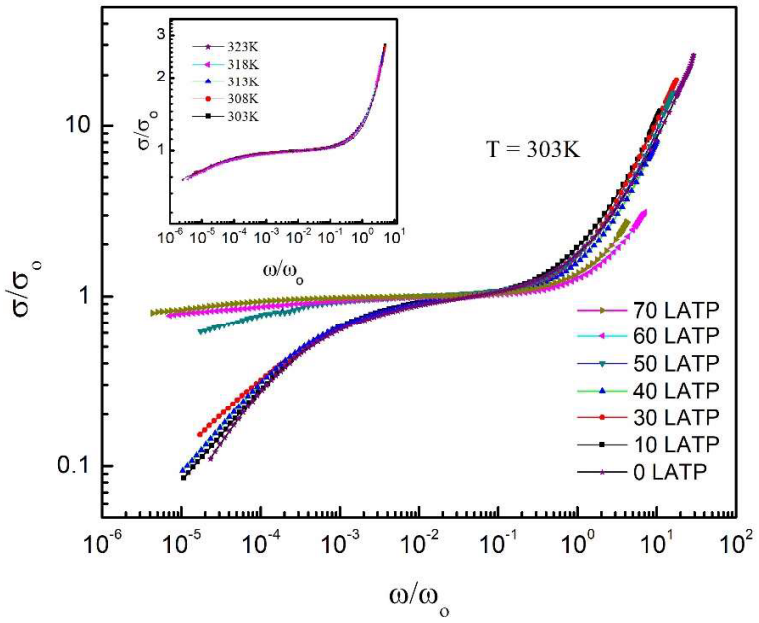

Figure 3.12 *Scaling behaviour of electrical conductivity at room temperature for CPEs 5LiCF3SO3-95[PEO1-xLATPx] where 0 ≤ x ≤ 0.7. Inset: 70 LATP composites with temperature.*

3.2.4 Ionic Transport number and mobility:

Since the salt content in these series of sample is fixed to 5 wt% of the composition, therefore it is of great significance to estimate how LATP presence in polymer matrix affects Li^+ ionic transport/transference number (as discussed in Chapter 2, section 2.4.8) along with ionic mobility (as discussed in Chapter 2, section 2.4.8) in the context of increase of conductivity (section 3.2.3).

A high frequency semicircle with a small diameter followed by a larger diameter semicircle (at lower frequencies) was seen in the Nyquist plots (Fig. 3.13a). This may be modeled as a

series combination of two parallel circuits of resistance (R) and constant phase element (CPE) as shown in the inset of Fig. 3.13a.

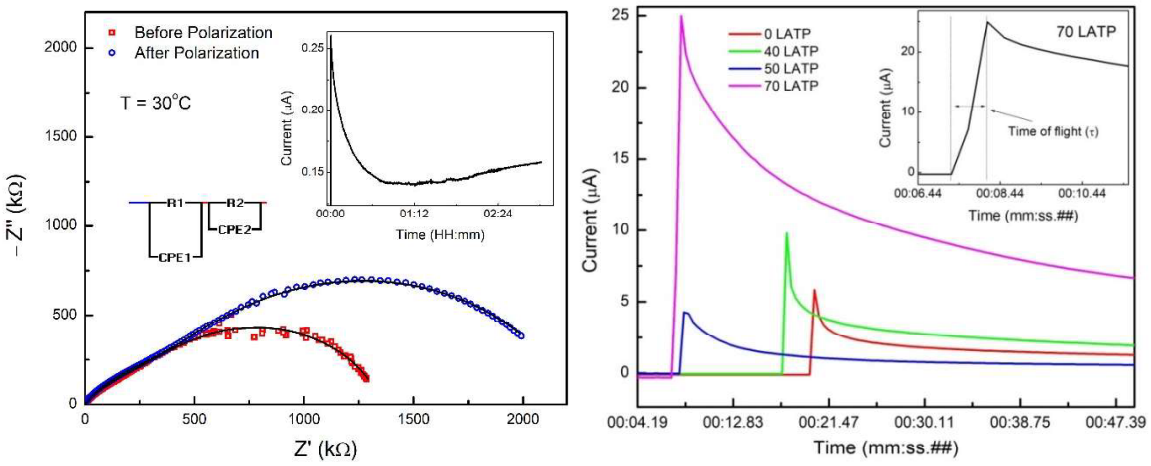

(a) (b)

Figure 3.13 *(a) Nyquist plots for Li|70LATP|Li cell configuration before and after polarization. Inset shows (i) corresponding equivalent circuit and (ii) polarization (ionic) current profile with time. (b) Transient ionic current during reversing of potential versus time for 0 LATP, 40 LATP, 50 LATP and 70 LATP in a cell configuration of Ag/sample/Ag. Inset shows an extended graph for 70 LATP sample.*

Thus R1 and R2 may be assigned to bulk and lithium passivation layer resistance, respectively. The value of passivation layer resistance (R2) before and after polarization (R_o and R_s, respectively) are thus obtained and used in Equation (Chapter 2, equation 16) for transport number calculation. The t_{Li+} values for 70 LATP (Fig. 6), 0 LATP, 40 LATP and 50 LATP are shown in Table 1. For 0 LTP, t_{Li+} value lies in the range for similar compositions reported earlier [19]. Interestingly, there is a systematic increasing trend in t_{Li+} with LATP addition.

The transient ionic current variation with time is shown in Fig. 3.13b for 0-70 LATP composites. An interesting trend is again observed where mobility for high LATP content is apparently high (Table 1). Almost ~ 2 orders of magnitude rise in the mobility is observed for 70 LATP sample in comparison to 0 LTP.

Table 3.1 *Calculated O/Li ratio, Li^+ ion transport number, and ionic mobility for 0-70 LATP composites.*

Composition	O/Li	Mobility (μ) cm^2/V- s	t +
0 LATP	67/1	$(1.9 \pm 0.2) \times 10^{-3}$	0.12 ± 0.5
40 LATP	40/1	$(2.0 \pm 0.2) \times 10^{-3}$	0.25 ± 0.5
50 LATP	33/1	$(3.5 \pm 0.2) \times 10^{-1}$	0.35 ± 0.5
70 LATP	20/1	$(2.0 \pm 0.2) \times 10^{-1}$	0.46 ± 0.5

3.3. Summary

(i) LTP, as well as LATP dispersed polymer composites could be prepared in a wide range of the composition. Samples were found to be embedded with evenly distributed active crystallite fillers of uniform size.

(ii) LATP/LTP addition suppresses the crystallization of PEO. For large filler content, thermal cycling stability notably improves at least up to 100°C.

(iii) Samples are predominantly ionic. Grain conductivity plays an important role. LATP filler gives improved conductivity.

(iv) LATP/LTP dispersion affects ion mobility particularly for large content of fillers.

(v) Ionic transport number interestingly changes with LATP addition. In fact, careful calculation suggests a systematic rise of t_{Li^+} with such reinforcement of active fillers that may be attributed to pathways provide by these crystallites. This in turn also suggests discouragement of anion transport due to active filler addition.

(vi)LATP/LTP addition certainly affects the mechanism of transport. A detailed investigation will be presented in chapter 5 where structural studies have been separately carried out to propose a transport mechanism.

References:

[1] S. K. Fullerton-Shirey, J. K. Maranas, *J. Phys. Chem. C* **2010**, *114*, 9196.

[2] S. K. Chaurasia, R. K. Singh, S. Chandra, *Solid State Ionics* **2014**, *262*, 790.

[3] H. El-Shinawi, J. Janek, *RSC Adv.* **2015**, *5*, 14887.

[4] E. Quartarone, *Solid State Ionics* **1998**, *110*, 1.

[5] K. S. Ngai, S. Ramesh, K. Ramesh, J. C. Juan, *Ionics (Kiel).* **2016**, DOI

10.1007/s11581-016-1756-4.

[6] F. Croce, G. B. Appetecchi, L. Persi, B. Scrosati, *Nature* **1998**, *394*, 456.

[7] P. Anantha, K. Hariharan, *Solid State Ionics* **2005**, *176*, 155.

[8] J. Płcharski, W. Weiczorek, *Solid State Ionics* **1988**, *28–30*, 979.

[9] B. G. Adachi, N. Imanaka, H. Aono, **1996**, 127.

[10] W. Bucheli, R. Jiménez, J. Sanz, A. Várez, *Solid State Ionics* **2012**, *227*, 113.

[11] R. Jimenez, A. Rivera, A. Varez, J. Sanz, *Solid State Ionics* **2009**, *180*, 1362.

[12] M. Kleitz, L. Dessemond, M. C. Steil, *Solid State Ionics* **1995**, *75*, 107.

[13] A. S. Best, M. Forsyth, D. R. Macfarlane, *Group* **2000**, *137*, 339.

[14] S. Wang, L. Ben, H. Li, L. Chen, *Solid State Ionics* **2014**, *268*, 110.

[15] T. Zangina, J. Hassan, K. A. Matori, R. S. Azis, U. Ahmadu, A. See, *Results Phys.* **2016**, *6*, 719.

[16] H. Aono, E. Sugimoto, Y. Sadaoka, N. Imanaka, G. ya Adachi, *Solid State Ionics* **1990**, *40–41*, 38.

[17] G. P. Pandey, S. A. Hashmi, R. C. Agrawal, *Solid State Ionics* **2008**, *179*, 543.

[18] H. Aono, E. Sugimoto, Y. Sadaoka, N. Imanaka, G. Adachi, *J. Electrochem. Soc.* **1990**, *137*, 1023.

[19] Y. Kato, M. Watanabe, K. Sanui, N. Ogata, *Solid State Ionics* **1990**, *40–41*, 632.